

Measurement of Time-Dependent CP -Violating Asymmetries and Constraints on $\sin(2\beta + \gamma)$ with Partial Reconstruction of $B \rightarrow D^{*\mp}\pi^\pm$ Decays

B. Aubert, R. Barate, D. Boutigny, F. Couderc, Y. Karyotakis, J. P. Lees, V. Poireau, V. Tisserand, and A. Zghiche
Laboratoire de Physique des Particules, F-74941 Annecy-le-Vieux, France

E. Grauges
IFAE, Universitat Autònoma de Barcelona, E-08193 Bellaterra, Barcelona, Spain

A. Palano, M. Pappagallo, and A. Pompili
Università di Bari, Dipartimento di Fisica and INFN, I-70126 Bari, Italy

J. C. Chen, N. D. Qi, G. Rong, P. Wang, and Y. S. Zhu
Institute of High Energy Physics, Beijing 100039, China

G. Eigen, I. Ofte, and B. Stugu
University of Bergen, Inst. of Physics, N-5007 Bergen, Norway

G. S. Abrams, M. Battaglia, A. W. Borgland, A. B. Breon, D. N. Brown, J. Button-Shafer, R. N. Cahn, E. Charles, C. T. Day, M. S. Gill, A. V. Gritsan, Y. Groysman, R. G. Jacobsen, R. W. Kadel, J. Kadyk, L. T. Kerth, Yu. G. Kolomensky, G. Kukartsev, G. Lynch, L. M. Mir, P. J. Oddone, T. J. Orimoto, M. Pripstein, N. A. Roe, M. T. Ronan, and W. A. Wenzel
Lawrence Berkeley National Laboratory and University of California, Berkeley, California 94720, USA

M. Barrett, K. E. Ford, T. J. Harrison, A. J. Hart, C. M. Hawkes, S. E. Morgan, and A. T. Watson
University of Birmingham, Birmingham, B15 2TT, United Kingdom

M. Fritsch, K. Goetzen, T. Held, H. Koch, B. Lewandowski, M. Pelizaeus, K. Peters, T. Schroeder, and M. Steinke
Ruhr Universität Bochum, Institut für Experimentalphysik 1, D-44780 Bochum, Germany

J. T. Boyd, J. P. Burke, N. Chevalier, W. N. Cottingham, and M. P. Kelly
University of Bristol, Bristol BS8 1TL, United Kingdom

T. Cuhadar-Donszelmann, C. Hearty, N. S. Knecht, T. S. Mattison, and J. A. McKenna
University of British Columbia, Vancouver, British Columbia, Canada V6T 1Z1

A. Khan, P. Kyberd, and L. Teodorescu
Brunel University, Uxbridge, Middlesex UB8 3PH, United Kingdom

A. E. Blinov, V. E. Blinov, A. D. Bukin, V. P. Druzhinin, V. B. Golubev, V. N. Ivanchenko, E. A. Kravchenko, A. P. Onuchin, S. I. Serednyakov, Yu. I. Skovpen, E. P. Solodov, and A. N. Yushkov
Budker Institute of Nuclear Physics, Novosibirsk 630090, Russia

D. Best, M. Bondioli, M. Bruinsma, M. Chao, I. Eschrich, D. Kirkby, A. J. Lankford, M. Mandelkern, R. K. Mommsen, W. Roethel, and D. P. Stoker
University of California at Irvine, Irvine, California 92697, USA

C. Buchanan, B. L. Hartfiel, and A. J. R. Weinstein
University of California at Los Angeles, Los Angeles, California 90024, USA

S. D. Foulkes, J. W. Gary, O. Long, B. C. Shen, K. Wang, and L. Zhang
University of California at Riverside, Riverside, California 92521, USA

D. del Re, H. K. Hadavand, E. J. Hill, D. B. MacFarlane, H. P. Paar, S. Rahatlou, and V. Sharma

University of California at San Diego, La Jolla, California 92093, USA

J. W. Berryhill, C. Campagnari, A. Cunha, B. Dahmes,
T. M. Hong, A. Lu, M. A. Mazur, J. D. Richman, and W. Verkerke
University of California at Santa Barbara, Santa Barbara, California 93106, USA

T. W. Beck, A. M. Eisner, C. J. Flacco, C. A. Heusch, J. Kroseberg, W. S. Lockman, G. Nesom,
T. Schalk, B. A. Schumm, A. Seiden, P. Spradlin, D. C. Williams, and M. G. Wilson
University of California at Santa Cruz, Institute for Particle Physics, Santa Cruz, California 95064, USA

J. Albert, E. Chen, G. P. Dubois-Felsmann, A. Dvoretzskii, D. G. Hitlin,
I. Narsky, T. Piatenko, F. C. Porter, A. Ryd, and A. Samuel
California Institute of Technology, Pasadena, California 91125, USA

R. Andreassen, S. Jayatilleke, G. Mancinelli, B. T. Meadows, and M. D. Sokoloff
University of Cincinnati, Cincinnati, Ohio 45221, USA

F. Blanc, P. Bloom, S. Chen, W. T. Ford, U. Nauenberg, A. Olivas, P. Rankin,
W. O. Ruddick, J. G. Smith, K. A. Ulmer, S. R. Wagner, and J. Zhang
University of Colorado, Boulder, Colorado 80309, USA

A. Chen, E. A. Eckhart, J. L. Harton, A. Soffer, W. H. Toki, R. J. Wilson, and Q. Zeng
Colorado State University, Fort Collins, Colorado 80523, USA

B. Spaan
Universität Dortmund, Institut für Physik, D-44221 Dortmund, Germany

D. Altenburg, T. Brandt, J. Brose, M. Dickopp, E. Feltresi, A. Hauke, V. Klose, H. M. Lacker, E. Maly,
R. Nogowski, S. Otto, A. Petzold, G. Schott, J. Schubert, K. R. Schubert, R. Schwierz, and J. E. Sundermann
Technische Universität Dresden, Institut für Kern- und Teilchenphysik, D-01062 Dresden, Germany

D. Bernard, G. R. Bonneaud, P. Grenier, S. Schrenk, Ch. Thiebaux, G. Vasileiadis, and M. Verderi
Ecole Polytechnique, LLR, F-91128 Palaiseau, France

D. J. Bard, P. J. Clark, W. Gradl, F. Muheim, S. Playfer, and Y. Xie
University of Edinburgh, Edinburgh EH9 3JZ, United Kingdom

M. Andreotti, V. Azzolini, D. Bettoni, C. Bozzi, R. Calabrese, G. Cibinetto, E. Luppi, M. Negrini, and L. Piemontese
Università di Ferrara, Dipartimento di Fisica and INFN, I-44100 Ferrara, Italy

F. Anulli, R. Baldini-Ferrolì, A. Calcaterra, R. de Sangro,
G. Finocchiaro, P. Patteri, I. M. Peruzzi, M. Piccolo, and A. Zallo
Laboratori Nazionali di Frascati dell'INFN, I-00044 Frascati, Italy

A. Buzzo, R. Capra, R. Contri, M. Lo Vetere, M. Macri, M. R. Monge,
S. Passaggio, C. Patrignani, E. Robutti, A. Santroni, and S. Tosi
Università di Genova, Dipartimento di Fisica and INFN, I-16146 Genova, Italy

S. Bailey, G. Brandenburg, K. S. Chaisanguanthum, M. Morii, and E. Won
Harvard University, Cambridge, Massachusetts 02138, USA

R. S. Dubitzky, U. Langenegger, J. Marks, S. Schenk, and U. Uwer
Universität Heidelberg, Physikalisches Institut, Philosophenweg 12, D-69120 Heidelberg, Germany

W. Bhimji, D. A. Bowerman, P. D. Dauncey, U. Egede, R. L. Flack,
J. R. Gaillard, G. W. Morton, J. A. Nash, M. B. Nikolich, and G. P. Taylor
Imperial College London, London, SW7 2AZ, United Kingdom

M. J. Charles, G. J. Grenier, U. Mallik, and A. K. Mohapatra
University of Iowa, Iowa City, Iowa 52242, USA

J. Cochran, H. B. Crawley, V. Eyges, W. T. Meyer, S. Prell, E. I. Rosenberg, A. E. Rubin, and J. Yi
Iowa State University, Ames, Iowa 50011-3160, USA

N. Arnaud, M. Davier, X. Giroux, G. Grosdidier, A. Höcker, F. Le Diberder, V. Lepeltier, A. M. Lutz, A. Oyanguren,
 T. C. Petersen, M. Pierini, S. Plaszczynski, S. Rodier, P. Roudeau, M. H. Schune, A. Stocchi, and G. Wormser
Laboratoire de l'Accélérateur Linéaire, F-91898 Orsay, France

C. H. Cheng, D. J. Lange, M. C. Simani, and D. M. Wright
Lawrence Livermore National Laboratory, Livermore, California 94550, USA

A. J. Bevan, C. A. Chavez, J. P. Coleman, I. J. Forster, J. R. Fry, E. Gabathuler,
 R. Gamet, K. A. George, D. E. Hutchcroft, R. J. Parry, D. J. Payne, and C. Touramanis
University of Liverpool, Liverpool L69 72E, United Kingdom

C. M. Cormack and F. Di Lodovico
Queen Mary, University of London, E1 4NS, United Kingdom

C. L. Brown, G. Cowan, H. U. Flaecher, M. G. Green, P. S. Jackson, T. R. McMahon, S. Ricciardi, and F. Salvatore
University of London, Royal Holloway and Bedford New College, Egham, Surrey TW20 0EX, United Kingdom

D. Brown and C. L. Davis
University of Louisville, Louisville, Kentucky 40292, USA

J. Allison, N. R. Barlow, R. J. Barlow, M. C. Hodgkinson, G. D. Lafferty, M. T. Naisbit, and J. C. Williams
University of Manchester, Manchester M13 9PL, United Kingdom

C. Chen, A. Farbin, W. D. Hulsbergen, A. Jawahery, D. Kovalskyi, C. K. Lae, V. Lillard, and D. A. Roberts
University of Maryland, College Park, Maryland 20742, USA

G. Blaylock, C. Dallapiccola, S. S. Hertzbach, R. Kofler, V. B. Koptchev,
 X. Li, T. B. Moore, S. Saremi, H. Staengle, and S. Willocq
University of Massachusetts, Amherst, Massachusetts 01003, USA

R. Cowan, K. Koeneke, G. Sciolla, S. J. Sekula, F. Taylor, and R. K. Yamamoto
Massachusetts Institute of Technology, Laboratory for Nuclear Science, Cambridge, Massachusetts 02139, USA

H. Kim, P. M. Patel, and S. H. Robertson
McGill University, Montréal, Quebec, Canada H3A 2T8

A. Lazzaro, V. Lombardo, and F. Palombo
Università di Milano, Dipartimento di Fisica and INFN, I-20133 Milano, Italy

J. M. Bauer, L. Cremaldi, V. Eschenburg, R. Godang, R. Kroeger,
 J. Reidy, D. A. Sanders, D. J. Summers, and H. W. Zhao
University of Mississippi, University, Mississippi 38677, USA

S. Brunet, D. Côté, P. Taras, and B. Viaud
Université de Montréal, Laboratoire René J. A. Lévesque, Montréal, Quebec, Canada H3C 3J7

H. Nicholson
Mount Holyoke College, South Hadley, Massachusetts 01075, USA

N. Cavallo,* G. De Nardo, F. Fabozzi,* C. Gatto, L. Lista, D. Monorchio, P. Paolucci, D. Piccolo, and C. Sciacca
Università di Napoli Federico II, Dipartimento di Scienze Fisiche and INFN, I-80126, Napoli, Italy

M. Baak, H. Bulten, G. Raven, H. L. Snoek, and L. Wilden
NIKHEF, National Institute for Nuclear Physics and High Energy Physics, NL-1009 DB Amsterdam, The Netherlands

C. P. Jessop and J. M. LoSecco
University of Notre Dame, Notre Dame, Indiana 46556, USA

T. Allmendinger, G. Benelli, K. K. Gan, K. Honscheid, D. Hufnagel, P. D. Jackson,
 H. Kagan, R. Kass, T. Pulliam, A. M. Rahimi, R. Ter-Antonyan, and Q. K. Wong
Ohio State University, Columbus, Ohio 43210, USA

J. Brau, R. Frey, O. Igonkina, M. Lu, C. T. Potter, N. B. Sinev, D. Strom, and E. Torrence
University of Oregon, Eugene, Oregon 97403, USA

F. Colecchia, A. Dorigo, F. Galeazzi, M. Margoni, M. Morandin,
 M. Posocco, M. Rotondo, F. Simonetto, R. Stroili, and C. Voci
Università di Padova, Dipartimento di Fisica and INFN, I-35131 Padova, Italy

M. Benayoun, H. Briand, J. Chauveau, P. David, L. Del Buono, Ch. de la Vaissière,
 O. Hamon, M. J. J. John, Ph. Leruste, J. Malclès, J. Ocariz, L. Roos, and G. Therin
Universités Paris VI et VII, Laboratoire de Physique Nucléaire et de Hautes Energies, F-75252 Paris, France

P. K. Behera, L. Gladney, Q. H. Guo, and J. Panetta
University of Pennsylvania, Philadelphia, Pennsylvania 19104, USA

M. Biasini, R. Covarelli, S. Pacetti, and M. Pioppi
Università di Perugia, Dipartimento di Fisica and INFN, I-06100 Perugia, Italy

C. Angelini, G. Batignani, S. Bettarini, F. Bucci, G. Calderini, M. Carpinelli, F. Forti, M. A. Giorgi,
 A. Lusiani, G. Marchiori, M. Morganti, N. Neri, E. Paoloni, M. Rama, G. Rizzo, G. Simi, and J. Walsh
Università di Pisa, Dipartimento di Fisica, Scuola Normale Superiore and INFN, I-56127 Pisa, Italy

M. Haire, D. Judd, K. Paick, and D. E. Wagoner
Prairie View A&M University, Prairie View, Texas 77446, USA

J. Biesiada, N. Danielson, P. Elmer, Y. P. Lau, C. Lu, J. Olsen, A. J. S. Smith, and A. V. Telnov
Princeton University, Princeton, New Jersey 08544, USA

F. Bellini, G. Cavoto, A. D'Orazio, E. Di Marco, R. Faccini, F. Ferrarotto, F. Ferroni, M. Gaspero,
 L. Li Gioi, M. A. Mazzoni, S. Morganti, G. Piredda, F. Polci, F. Safai Tehrani, and C. Voena
Università di Roma La Sapienza, Dipartimento di Fisica and INFN, I-00185 Roma, Italy

S. Christ, H. Schröder, G. Wagner, and R. Waldi
Universität Rostock, D-18051 Rostock, Germany

T. Adye, N. De Groot, B. Franek, G. P. Gopal, E. O. Olaiya, and F. F. Wilson
Rutherford Appleton Laboratory, Chilton, Didcot, Oxon, OX11 0QX, United Kingdom

R. Aleksan, S. Emery, A. Gaidot, S. F. Ganzhur, P.-F. Giraud, G. Graziani, G. Hamel de Monchenault,
 W. Kozanecki, M. Legendre, G. W. London, B. Mayer, G. Vasseur, Ch. Yèche, and M. Zito
DSM/Dapnia, CEA/Saclay, F-91191 Gif-sur-Yvette, France

M. V. Purohit, A. W. Weidemann, J. R. Wilson, and F. X. Yumiceva
University of South Carolina, Columbia, South Carolina 29208, USA

T. Abe, M. T. Allen, D. Aston, R. Bartoldus, N. Berger, A. M. Boyarski, O. L. Buchmueller, R. Claus,
 M. R. Convery, M. Cristinziani, J. C. Dingfelder, D. Dong, J. Dorfan, D. Dujmic, W. Dunwoodie, S. Fan,
 R. C. Field, T. Glanzman, S. J. Gowdy, T. Hadig, V. Halyo, C. Hast, T. Hryn'ova, W. R. Innes, M. H. Kelsey,

P. Kim, M. L. Kocian, D. W. G. S. Leith, J. Libby, S. Luitz, V. Luth, H. L. Lynch, H. Marsiske, R. Messner, D. R. Muller, C. P. O'Grady, V. E. Ozcan, A. Perazzo, M. Perl, B. N. Ratcliff, A. Roodman, A. A. Salnikov, R. H. Schindler, J. Schwiening, A. Snyder, J. Stelzer, D. Su, M. K. Sullivan, K. Suzuki, J. M. Thompson, J. Va'vra, M. Weaver, W. J. Wisniewski, M. Wittgen, D. H. Wright, A. K. Yarritu, K. Yi, and C. C. Young
Stanford Linear Accelerator Center, Stanford, California 94309, USA

J. Strube
*University of Oregon, Eugene, Oregon 97403, USA and
Stanford Linear Accelerator Center, Stanford, California 94309, USA*

P. R. Burchat, A. J. Edwards, S. A. Majewski, B. A. Petersen, and C. Roat
Stanford University, Stanford, California 94305-4060, USA

M. Ahmed, S. Ahmed, M. S. Alam, J. A. Ernst, M. A. Saeed, M. Saleem, F. R. Wappler, and S. B. Zain
State University of New York, Albany, New York 12222, USA

W. Bugg, M. Krishnamurthy, and S. M. Spanier
University of Tennessee, Knoxville, Tennessee 37996, USA

R. Eckmann, J. L. Ritchie, A. Satpathy, and R. F. Schwitters
University of Texas at Austin, Austin, Texas 78712, USA

J. M. Izen, I. Kitayama, X. C. Lou, and S. Ye
University of Texas at Dallas, Richardson, Texas 75083, USA

F. Bianchi, M. Bona, F. Gallo, and D. Gamba
Università di Torino, Dipartimento di Fisica Sperimentale and INFN, I-10125 Torino, Italy

M. Bomben, L. Bosisio, C. Cartaro, F. Cossutti, G. Della Ricca, S. Dittongo,
S. Grancagnolo, L. Lanceri, P. Poropat,[†] L. Vitale, and G. Vuagnin
Università di Trieste, Dipartimento di Fisica and INFN, I-34127 Trieste, Italy

F. Martinez-Vidal
IFIC, Universitat de Valencia-CSIC, E-46071 Valencia, Spain

R. S. Panvini[†]
Vanderbilt University, Nashville, Tennessee 37235, USA

Sw. Banerjee, B. Bhuyan, C. M. Brown, D. Fortin, K. Hamano, R. Kowalewski, J. M. Roney, and R. J. Sobie
University of Victoria, Victoria, British Columbia, Canada V8W 3P6

J. J. Back, P. F. Harrison, T. E. Latham, and G. B. Mohanty
Department of Physics, University of Warwick, Coventry CV4 7AL, United Kingdom

H. R. Band, X. Chen, B. Cheng, S. Dasu, M. Datta, A. M. Eichenbaum, K. T. Flood,
M. Graham, J. J. Hollar, J. R. Johnson, P. E. Kutter, H. Li, R. Liu, B. Mellado, A. Mihalys,
Y. Pan, R. Prepost, P. Tan, J. H. von Wimmersperg-Toeller, J. Wu, S. L. Wu, and Z. Yu
University of Wisconsin, Madison, Wisconsin 53706, USA

M. G. Greene and H. Neal
Yale University, New Haven, Connecticut 06511, USA

(Dated: July 3, 2018)

We present a measurement of the time-dependent CP -violating asymmetries in decays of neutral B mesons to the final states $D^{*\mp}\pi^\pm$, using approximately 232 million $B\bar{B}$ events recorded by the BABAR experiment at the PEP-II e^+e^- storage ring. Events containing these decays are selected with a partial reconstruction technique, in which only the high-momentum π^\pm from the B decay and the low-momentum π^\mp from the $D^{*\mp}$ decay are used. We measure the parameters related to $2\beta + \gamma$ to be $a_{D^*\pi} = -0.034 \pm 0.014 \pm 0.009$ and $c_{D^*\pi}^\ell = -0.019 \pm 0.022 \pm 0.013$. With some theoretical

assumptions, we interpret our results in terms of the lower limits $|\sin(2\beta + \gamma)| > 0.62$ (0.35) at 68% (90%) confidence level.

PACS numbers: 13.25.Hw, 12.15.Hh, 11.30.Er

I. INTRODUCTION

The Cabibbo-Kobayashi-Maskawa (CKM) quark-mixing matrix [1] provides an explanation of CP violation and is under experimental investigation aimed at constraining its parameters. A crucial part of this program is the measurement of the angle $\gamma = \arg(-V_{ud}V_{ub}^*/V_{cd}V_{cb}^*)$ of the unitarity triangle related to the CKM matrix. The decay modes $B \rightarrow D^{*\mp}\pi^\pm$ have been proposed for use in measurements of $\sin(2\beta + \gamma)$ [2], where $\beta = \arg(-V_{cd}V_{cb}^*/V_{td}V_{tb}^*)$ is well measured [3]. In the Standard Model the decays $B^0 \rightarrow D^{*-}\pi^+$ and $\bar{B}^0 \rightarrow D^{*-}\pi^+$ proceed through the $\bar{b} \rightarrow \bar{c}u\bar{d}$ and $b \rightarrow u\bar{c}d$ amplitudes A_c and A_u . Fig. 1 shows the tree diagrams contributing to these decays. The relative weak phase between A_u and A_c in the usual Wolfenstein convention [4] is γ . When combined with $B^0\bar{B}^0$ mixing, this yields a weak phase difference of $2\beta + \gamma$ between the interfering amplitudes.

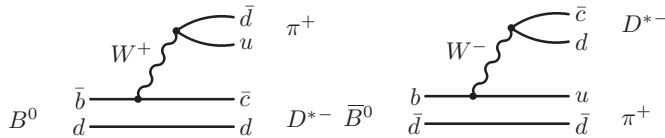


FIG. 1: Feynman diagrams for the Cabibbo-favored decay $B^0 \rightarrow D^{*-}\pi^+$ (left), corresponding to the decay amplitude A_c , and the Cabibbo-suppressed decay $\bar{B}^0 \rightarrow D^{*-}\pi^+$ (right), whose amplitude is A_u .

In $\Upsilon(4S) \rightarrow B\bar{B}$ decays, the decay rate distribution for $B \rightarrow D^{*\mp}\pi^\pm$ is

$$\mathcal{P}_\eta^\pm(\Delta t) = \frac{e^{-|\Delta t|/\tau}}{4\tau} \times [1 \mp S^\zeta \sin(\Delta m \Delta t) \mp \eta C \cos(\Delta m \Delta t)], \quad (1)$$

where τ is the B^0 lifetime averaged over the two mass eigenstates, Δm is the $B^0\bar{B}^0$ mixing frequency, and Δt is the difference between the time of the $B \rightarrow D^{*\mp}\pi^\pm$ (B_{rec}) decay and the decay of the other B (B_{tag}) in the event. The upper (lower) signs in Eq. (1) indicate the flavor of the B_{tag} as a B^0 (\bar{B}^0), while $\eta = +1$ (-1) and $\zeta = +$ ($-$) for the B_{rec} final state $D^{*-}\pi^+$ ($D^{*+}\pi^-$). The parameters C and S^\pm are given by

$$C \equiv \frac{1 - r^{*2}}{1 + r^{*2}}, \quad S^\pm \equiv \frac{2r^*}{1 + r^{*2}} \sin(2\beta + \gamma \pm \delta^*). \quad (2)$$

Here δ^* is the strong phase difference between A_u and A_c , and $r^* = |A_u/A_c|$. Since A_u is doubly CKM-suppressed with respect to A_c , one expects $r^* \approx \left| \frac{V_{ub}V_{cd}^*}{V_{cb}V_{ud}^*} \right| = 0.02$.

We report a study of the CP -violating asymmetry in $B \rightarrow D^{*\mp}\pi^\pm$ decays using the technique of partial reconstruction, which allows us to achieve a high efficiency for the selection of signal events. We use approximately twice the integrated luminosity of our previous analysis of this process [5], and employ an improved method to eliminate a measurement bias, as described in Sec. III F 2. Many of the tools and procedures used in this analysis were validated in a previous analysis dedicated to the measurement of the B^0 lifetime [6].

In this analysis, terms of order r^{*2} , to which we currently have no sensitivity, have been neglected. The interpretation of the measured asymmetries in terms of $\sin(2\beta + \gamma)$ requires an assumption regarding the value of r^* , discussed in Sec. VI.

II. THE BABAR DETECTOR AND DATASET

The data used in this analysis were recorded with the BABAR detector at the PEP-II asymmetric-energy storage rings, and consist of 211 fb^{-1} collected on the $\Upsilon(4S)$ resonance (on-resonance sample), and 21 fb^{-1} collected at an e^+e^- center-of-mass (CM) energy approximately 40 MeV below the resonance peak (off-resonance sample). Samples of Monte Carlo (MC) [7] events with an equivalent luminosity approximately four times larger than the data sample were analyzed using the same reconstruction and analysis procedure.

The BABAR detector is described in detail in Ref. [8]. We provide a brief description of the main components and their use in this analysis. Charged-particle trajectories are measured by a combination of a five-layer silicon vertex tracker (SVT) and a 40-layer drift chamber (DCH) in a 1.5-T solenoidal magnetic field. Tracks with low transverse momentum can be reconstructed in the SVT alone, thus extending the charged-particle detection down to transverse momenta of about 50 MeV/c. We use a ring-imaging Cherenkov detector (DIRC) for charged-particle identification and augment it with energy-loss measurements from the SVT and DCH. Photons and electrons are detected in a CsI(Tl) electromagnetic calorimeter (EMC), with photon-energy resolution $\sigma_E/E = 0.023(E/\text{GeV})^{-1/4} \oplus 0.014$. The instrumented flux return (IFR) is equipped with resistive plate chambers to identify muons.

*Also with Università della Basilicata, Potenza, Italy

†Deceased

III. ANALYSIS METHOD

A. Partial Reconstruction of $B \rightarrow D^{*\mp}\pi^\pm$

In the partial reconstruction of a $B \rightarrow D^{*\mp}\pi^\pm$ candidate (B_{rec}), only the hard (high-momentum) pion track π_h from the B decay and the soft (low-momentum) pion track π_s from the decay $D^{*-} \rightarrow \bar{D}^0\pi_s^-$ are used. The cosine of the angle between the momenta of the B and the hard pion in the CM frame is then computed:

$$\cos\theta_{Bh} = \frac{M_{D^{*-}}^2 - M_{B^0}^2 - M_\pi^2 + E_{\text{CM}}E_h}{2p_B|\vec{p}_h|}, \quad (3)$$

where M_x is the nominal mass of particle x [9], E_h and \vec{p}_h are the measured CM energy and momentum of the hard pion, E_{CM} is the total CM energy of the incoming e^+e^- beams, and $p_B = \sqrt{E_{\text{CM}}^2/4 - M_{B^0}^2}$. Events are required to be in the physical region $|\cos\theta_{Bh}| < 1$. Given $\cos\theta_{Bh}$ and the measured momenta of the π_h and π_s , the B four-momentum can be calculated up to an unknown azimuthal angle ϕ around \vec{p}_h . For every value of ϕ , the expected D four-momentum $p_D(\phi)$ is determined from four-momentum conservation, and the corresponding ϕ -dependent invariant mass $m(\phi) \equiv \sqrt{|p_D(\phi)|^2}$ is calculated. We define the missing mass $m_{\text{miss}} \equiv \frac{1}{2}[m_{\text{max}} + m_{\text{min}}]$, where m_{max} and m_{min} are the maximum and minimum values of $m(\phi)$. In signal events, m_{miss} peaks at the nominal D^0 mass M_{D^0} , with a gaussian width of about 3 MeV/ c^2 (Fig. 2). The m_{miss} distribution for combinatoric background events is significantly broader, making the missing mass the primary variable for distinguishing signal from background. The discrimination between signal and background provided by the m_{miss} distribution is independent of the choice of the value of ϕ . With the arbitrary choice $\phi = 0$, we use four-momentum conservation to calculate the CM D and B momentum vectors, which are used as described below.

B. Backgrounds

In addition to $B \rightarrow D^{*\mp}\pi^\pm$ events, the selected event sample contains the following kinds of events:

- $B \rightarrow D^{*\mp}\rho^\pm$.
- Peaking $B\bar{B}$ background, defined as decays other than $B \rightarrow D^{*\mp}\rho^\pm$, in which the π_h and π_s originate from the same B meson, with the π_s originating from a charged D^* decay. The m_{miss} distribution of these events peaks broadly under the signal peak.
- Combinatoric $B\bar{B}$ background, defined as all remaining $B\bar{B}$ background events.
- Continuum $e^+e^- \rightarrow q\bar{q}$, where q represents a u , d , s , or c quark.

C. Event Selection

To suppress the continuum background, we select events in which the ratio of the 2nd to the 0th Fox-Wolfram moment [10], computed using all charged particles and EMC clusters not matched to tracks, is smaller than 0.40. Hard-pion candidates are required to be reconstructed with at least twelve DCH hits. Kaons and leptons are rejected from the π_h candidate lists based on information from the IFR and DIRC, energy loss in the SVT and DCH, or the ratio of the candidate's EMC energy deposition to its momentum (E/p).

We define the D^* helicity angle θ_{D^*} to be the angle between the flight directions of the D and the B in the D^* rest frame. Taking advantage of the longitudinal polarization in signal events, we suppress background by requiring $|\cos\theta_{D^*}|$ to be larger than 0.4.

All candidates are required to satisfy $m_{\text{miss}} > 1.81 \text{ GeV}/c^2$. Multiple candidates are found in 5% of the events. In these instances, only the candidate with the m_{miss} value closest to M_{D^0} is used.

D. Fisher Discriminant

To further discriminate against continuum events, we combine fifteen event-shape variables into a Fisher discriminant [11] F . Discrimination originates from the fact that $q\bar{q}$ events tend to be jet-like, whereas $B\bar{B}$ events have a more spherical energy distribution. Rather than applying requirements to the variable F , we maximize the sensitivity by using it in the fits described below. The fifteen variables are calculated using two sets of particles. Set 1 includes all tracks and EMC clusters, excluding the hard and soft pion candidates; Set 2 is composed of Set 1, excluding all tracks and clusters with CM momentum within 1.25 radian of the CM momentum of the D . The variables, all calculated in the CM frame, are 1) the scalar sum of the momenta of all Set 1 tracks and EMC clusters in nine 20° angular bins centered about the hard pion direction; 2) the value of the sphericity, computed with Set 1; 3) the angle with respect to the hard pion of the sphericity axis, computed with Set 2; 4) the direction of the particle of highest energy in Set 2 with respect to the hard pion; 5) the absolute value of the vector sum of the momenta of all the particles in Set 2; 6) the momentum $|\vec{p}_h|$ of the hard pion and its polar angle.

E. Decay Time Measurement and Flavor Tagging

To perform this analysis, Δt and the flavor of the B_{tag} must be determined. We tag the flavor of the B_{tag} using lepton or kaon candidates. The lepton CM momentum is required to be greater than 1.1 GeV/ c to suppress leptons that originate from charm decays. If several flavor-tagging tracks are present in either the lepton or kaon tagging category, the only track of that category used for

tagging is the one with the largest value of θ_T , the CM angle between the track momentum and the momentum of the “missing” (unreconstructed) D . The tagging track must satisfy $\cos\theta_T < C_T$, where $C_T = 0.75$ ($C_T = 0.50$) for leptons (kaons), to minimize the impact of tracks originating from the decay of the missing D . If both a lepton and a kaon satisfy this requirement, the event is tagged with the lepton.

We measure Δt using $\Delta t = (z_{\text{rec}} - z_{\text{tag}})/(\gamma\beta c)$, where z_{rec} (z_{tag}) is the decay position of the B_{rec} (B_{tag}) along the beam axis (z) in the laboratory frame, and the e^+e^- boost parameter $\gamma\beta$ is calculated from the measured beam energies. To find z_{rec} , we use the π_h track parameters and errors, and the measured beam-spot position and size in the plane perpendicular to the beams (the $x-y$ plane). We find the position of the point in space for which the sum of the χ^2 contributions from the π_h track and the beam spot is a minimum. The z coordinate of this point determines z_{rec} . The beam spot has an r.m.s. size of approximately $120\ \mu\text{m}$ in the horizontal dimension (x), $5\ \mu\text{m}$ in the vertical dimension (y), and $8.5\ \text{mm}$ along the beams (z). The average B flight in the $x-y$ plane is $30\ \mu\text{m}$. To account for the B flight in the beam-spot-constrained vertex fit, $30\ \mu\text{m}$ are added to the effective x and y sizes for the purpose of conducting this fit.

In lepton-tagged events, the same procedure, with the π_h track replaced by the tagging lepton, is used to determine z_{tag} .

In kaon-tagged events, we obtain z_{tag} from a beam-spot-constrained vertex fit of all tracks in the event, excluding π_h , π_s and all tracks within 1 radian of the D momentum in the CM frame. If the contribution of any track to the χ^2 of the vertex is more than 6, the track is removed and the fit is repeated until no track fails the $\chi^2 < 6$ requirement.

The Δt error $\sigma_{\Delta t}$ is calculated from the results of the z_{rec} and z_{tag} vertex fits. We require $|\Delta t| < 15\ \text{ps}$ and $\sigma_{\Delta t} < 2\ \text{ps}$.

F. Probability Density Function

The probability density function (PDF) depends on the variables m_{miss} , Δt , $\sigma_{\Delta t}$, F , s_t , and s_m , where $s_t = 1$ (-1) when the B_{tag} is identified as a B^0 (\bar{B}^0), and $s_m = 1$ (-1) for “unmixed” (“mixed”) events. An event is labeled unmixed if the π_h is a π^- (π^+) and the B_{tag} is a B^0 (\bar{B}^0), and mixed otherwise.

The PDF for on-resonance data is a sum over the PDFs of the different event types:

$$\mathcal{P} = \sum_i f_i \mathcal{P}_i, \quad (4)$$

where the index $i = \{D^*\pi, D^*\rho, \text{peak}, \text{comb}, q\bar{q}\}$ indicates one of the event types described above, f_i is the relative fraction of events of type i in the data sample, and \mathcal{P}_i

is the PDF for these events. The PDF for off-resonance data is $\mathcal{P}_{q\bar{q}}$. The parameter values for \mathcal{P}_i are different for each event type, unless indicated otherwise. Each \mathcal{P}_i is a product,

$$\mathcal{P}_i = \mathcal{M}_i(m_{\text{miss}}) \mathcal{F}_i(F) \mathcal{T}'_i(\Delta t, \sigma_{\Delta t}, s_t, s_m), \quad (5)$$

where the factors in Eq. (5) are described below.

1. m_{miss} and F PDFs

The m_{miss} PDF for each event type i is the sum of a bifurcated Gaussian plus an ARGUS function [12]:

$$\mathcal{M}_i(m_{\text{miss}}) = f_i^{\hat{\mathcal{G}}} \hat{\mathcal{G}}_i(m_{\text{miss}}) + (1 - f_i^{\hat{\mathcal{G}}}) \mathcal{A}_i(m_{\text{miss}}), \quad (6)$$

where $f_i^{\hat{\mathcal{G}}}$ is the fractional area of the bifurcated Gaussian function. The functions $\hat{\mathcal{G}}_i$ and \mathcal{A}_i are

$$\hat{\mathcal{G}}_i(m) \propto \begin{cases} \exp[-(m - M_i)^2/2\sigma_{Li}^2] & , m \leq M_i \\ \exp[-(m - M_i)^2/2\sigma_{Ri}^2] & , m > M_i \end{cases}, \quad (7)$$

$$\mathcal{A}(m) \propto m \sqrt{1 - (m/M_i^A)^2} \times \exp\left[\epsilon_i \left(1 - (m/M_i^A)^2\right)\right] \theta(M_i^A - m), \quad (8)$$

where M_i is the peak of the bifurcated Gaussian, σ_{Li} and σ_{Ri} are its left and right widths, ϵ_i is the ARGUS exponent, M_i^A is its end point, and θ is the step function. The proportionality constants are such that each of these functions is normalized to unit area within the m_{miss} range. The m_{miss} PDF of each event type has different parameter values.

The Fisher discriminant PDF \mathcal{F}_i for each event type is parameterized as the sum of two Gaussians. The parameter values of $\mathcal{F}_{D^*\pi}$, $\mathcal{F}_{D^*\rho}$, $\mathcal{F}_{\text{peak}}$, and $\mathcal{F}_{\text{comb}}$ are identical.

2. Signal Δt PDFs

The Δt PDF $\mathcal{T}'_{D^*\pi}(\Delta t, \sigma_{\Delta t}, s_t, s_m)$ for signal events corresponds to Eq. 1 with $O(r^{*2})$ terms neglected, modified to account for several experimental effects, described below.

The first effect has to do with the origin of the tagging track. In some of the events, the tagging track originates from the decay of the missing D . These events are labeled “missing- D tags” and do not provide any information regarding the flavor of the B_{tag} . In lepton-tagged events, we further distinguish between “direct” tags, in which the tagging lepton originates directly from the decay of the B_{tag} , and “cascade” tags, where the tagging lepton is a daughter of a charmed particle produced in the B_{tag} decay. Due to the different physical origin of the tagging track in cascade and direct tags, these two event categories have different mistag probabilities, defined as the probability to deduce the wrong B flavor from the charge

of the tagging track. In addition, the measured value of z_{tag} in cascade-lepton tags is systematically larger than the true value, due to the finite lifetime of the charmed particle and the boosted CM frame. This creates a correlation between the tag and vertex measurements that we address by considering cascade-lepton tags separately in the PDF. In our previous analysis [5] we corrected for the bias of the S^\pm parameters caused by this effect and included a systematic error due to its uncertainty. In kaon tags, z_{tag} is determined using all available B_{tag} tracks, so the effect of the tagging track on the z_{tag} measurement is small. Therefore, the overall bias induced by cascade-kaon tags is small, and there is no need to distinguish them in the PDF.

The second experimental effect is the finite detector resolution in the measurement of Δt . We address this by convoluting the distribution of the true decay time difference Δt_{tr} with a detector resolution function. Putting these two effects together, the Δt PDF of signal events is

$$\mathcal{T}'_{D^*\pi}(\Delta t, \sigma_{\Delta t}, s_t, s_m) = (1 + s_t \Delta\epsilon_{D^*\pi}) \sum_j f_{D^*\pi}^j \times \int d\Delta t_{\text{tr}} \mathcal{T}_{D^*\pi}^j(\Delta t_{\text{tr}}, s_t, s_m) \mathcal{R}_{D^*\pi}^j(\Delta t - \Delta t_{\text{tr}}, \sigma_{\Delta t}), \quad (9)$$

where $\Delta\epsilon_{D^*\pi}$ is half the relative difference between the detection efficiencies of positive and negative leptons or kaons, the index $j = \{\text{dir}, \text{cas}, \text{miss}\}$ indicates direct, cascade, and missing- D tags, and $f_{D^*\pi}^j$ is the fraction of signal events of tag-type j in the sample. We set $f_{D^*\pi}^{\text{dir}} = 1 - f_{D^*\pi}^{\text{cas}} - f_{D^*\pi}^{\text{miss}}$ for lepton tags, with the value $f_{D^*\pi}^{\text{cas}} = 0.12 \pm 0.02$ obtained from the MC simulation. For kaon tags $f_{D^*\pi}^{\text{dir}} = 0$. The function $\mathcal{T}_{D^*\pi}^j(\Delta t_{\text{tr}}, s_t, s_m)$ is the Δt_{tr} distribution of tag-type j events, and $\mathcal{R}_{D^*\pi}^j(\Delta t - \Delta t_{\text{tr}}, \sigma_{\Delta t})$ is their resolution function, which parameterizes both the finite detector resolution and systematic offsets in the measurement of Δz , such as those due to the origin of the tagging particle. The parameterization of the resolution function is described in Sec. III F 4.

The functional form of the direct and cascade tag Δt_{tr} PDFs is

$$\mathcal{T}_{D^*\pi}^j(\Delta t_{\text{tr}}, s_t, s_m) = \frac{e^{-|\Delta t_{\text{tr}}|/\tau_{D^*\pi}}}{4\tau_{D^*\pi}} \times \left\{ 1 - s_t \Delta\omega_{D^*\pi}^j + s_m (1 - 2\omega_{D^*\pi}^j) \cos(\Delta m_{D^*\pi} \Delta t_{\text{tr}}) - \mathcal{S}_{D^*\pi}^j \sin(\Delta m_{D^*\pi} \Delta t_{\text{tr}}) \right\}, \quad (10)$$

where $j = \{\text{dir}, \text{cas}\}$, the mistag rate $\omega_{D^*\pi}^j$ is the probability to misidentify the flavor of the B_{tag} averaged over B^0 and \bar{B}^0 , and $\Delta\omega_{D^*\pi}^j$ is the B^0 mistag rate minus the \bar{B}^0 mistag rate. The factor $\mathcal{S}_{D^*\pi}^j$ describes the effect of interference between $b \rightarrow u\bar{c}d$ and $b \rightarrow c\bar{u}d$ amplitudes in

both the B_{rec} and the B_{tag} decays:

$$\mathcal{S}_{D^*\pi}^j = (1 - 2\omega_{D^*\pi}^j) (s_t a_{D^*\pi} + s_m c_{D^*\pi}) + s_t s_m b_{D^*\pi} (1 - s_t \Delta\omega_{D^*\pi}^j), \quad (11)$$

where $a_{D^*\pi}$, $b_{D^*\pi}$, and $c_{D^*\pi}$ are related to the physical parameters through

$$\begin{aligned} a_{D^*\pi} &\equiv 2r^* \sin(2\beta + \gamma) \cos\delta^*, \\ b_{D^*\pi} &\equiv 2r' \sin(2\beta + \gamma) \cos\delta', \\ c_{D^*\pi} &\equiv 2 \cos(2\beta + \gamma) (r^* \sin\delta^* - r' \sin\delta'), \end{aligned} \quad (12)$$

and r' (δ') is the effective magnitude of the ratio (effective strong phase difference) between the $b \rightarrow u\bar{c}d$ and $b \rightarrow c\bar{u}d$ amplitudes in the B_{tag} decay. This parameterization is good to first order in r^* and r' . In the following we will refer to the parameters $a_{D^*\pi}$, $b_{D^*\pi}$, $c_{D^*\pi}$ and related parameters for the background PDF as the weak phase parameters. Only $a_{D^*\pi}$ and $b_{D^*\pi}$ are related to CP violation, while $c_{D^*\pi}$ can be non-zero even in the absence of CP violation when $2\beta + \gamma = 0$. The inclusion of r' and δ' in the formalism accounts for cases where the B_{tag} undergoes a $b \rightarrow u\bar{c}d$ decay, and the kaon produced in the subsequent charm decay is used for tagging [13]. We expect $r' \sim 0.02$. In lepton-tagged events $r' = 0$ (and hence $b_{D^*\pi} = 0$) because most of the tagging leptons come from B semileptonic decays to which no suppressed amplitude with a different weak phase can contribute.

The Δt_{tr} PDF for missing- D tags is

$$\mathcal{T}_{D^*\pi}^{\text{miss}}(\Delta t_{\text{tr}}, s_t, s_m) = \frac{e^{-|\Delta t_{\text{tr}}|/\tau_{D^*\pi}^{\text{miss}}}}{8\tau_{D^*\pi}^{\text{miss}}} \left\{ 1 + s_m (1 - 2\rho_{D^*\pi}) - 2s_t s_m b_{D^*\pi} \sin(\Delta m_{D^*\pi} \Delta t_{\text{tr}}) \right\}, \quad (13)$$

where $\rho_{D^*\pi}$ is the probability that the charge of the tagging track is such that it results in a mixed flavor measurement. In this analysis, we have neglected the term proportional to $\sin(\Delta m_{D^*\pi} \Delta t_{\text{tr}})$ of Eq. 13. The systematic error on $b_{D^*\pi}$ due to this approximation is negligible due to the small value of $f_{D^*\pi}^{\text{miss}}$ reported below.

3. Background Δt PDFs

The Δt PDF of $B \rightarrow D^{*\mp} \rho^\pm$ has the same functional form and parameter values as the signal PDF, except that the weak phase parameters $a_{D^*\rho}$, $b_{D^*\rho}$, and $c_{D^*\rho}$ are set to 0 and are later varied to evaluate systematic uncertainties. The validity of the use of the same parameters for $\mathcal{T}_{D^*\rho}'$ and $\mathcal{T}_{D^*\pi}'$ is established using simulated events, and stems from the fact that the π_h momentum spectrum in the $B \rightarrow D^{*\mp} \rho^\pm$ events that pass our selection criteria is almost identical to the signal spectrum.

The Δt PDF of the peaking background accounts sep-

arately for charged and neutral B decays:

$$\begin{aligned} \mathcal{T}'_{\text{peak}}(\Delta t, \sigma_{\Delta t}, s_t, s_m) &= (1 + s_t \Delta \epsilon_{\text{peak}}) \left\{ \mathcal{T}'_{\text{peak}}{}^{0'} \right. \\ &+ \int d\Delta t_{\text{tr}} \mathcal{T}_{\text{peak}}^+(\Delta t_{\text{tr}}, s_t, s_m) \times \\ &\left. \mathcal{R}_{\text{peak}}^+(\Delta t - \Delta t_{\text{tr}}, \sigma_{\Delta t}) \right\}, \end{aligned} \quad (14)$$

where $\mathcal{T}'_{\text{peak}}{}^{0'}$ has the functional form of Eq. (9) and the subsequent expressions, Eqs. (13-12), but with all $D^*\pi$ -subscripted parameters replaced with their peak-subscripted counterparts. The integral in Eq. (14) accounts for the contribution of charged B decays to the peaking background, with

$$\mathcal{T}_{\text{peak}}^+(\Delta t_{\text{tr}}, s_t) = \frac{e^{-|\Delta t_{\text{tr}}|/\tau_{\text{peak}}^+}}{4\tau_{\text{peak}}^+} \left(1 - s_t \Delta \omega_{\text{peak}}^+ \right), \quad (15)$$

and $\mathcal{R}_{\text{peak}}^+(\Delta t - \Delta t_{\text{tr}}, \sigma_{\Delta t})$ being the three-Gaussian resolution function for these events described below.

The Combinatoric $B\bar{B}$ background PDF $\mathcal{T}'_{\text{comb}}$ is similar to the signal PDF, with one substantial difference. Instead of parameterizing $\mathcal{T}'_{\text{comb}}$ with the four parameters $f_{\text{comb}}^{\text{dir}}$, $\omega_{\text{comb}}^{\text{dir}}$, $\Delta \omega_{\text{comb}}^{\text{dir}}$, ρ_{comb} , we use the set of three parameters

$$\begin{aligned} \omega'_{\text{comb}} &= \omega_{\text{comb}}^{\text{dir}} (1 - f_{\text{comb}}^{\text{dir}}) + \frac{f_{\text{comb}}^{\text{dir}}}{2}, \\ \Delta \omega'_{\text{comb}} &= \Delta \omega_{\text{comb}} (1 - f_{\text{comb}}^{\text{dir}}), \\ \Omega_{\text{comb}} &= f_{\text{comb}}^{\text{dir}} (1 - 2\rho_{\text{comb}}). \end{aligned} \quad (16)$$

With these parameters and $f_{\text{comb}}^{\text{cas}} = 0$, the combinatoric $B\bar{B}$ background Δt PDF becomes

$$\begin{aligned} \mathcal{T}'_{\text{comb}}(\Delta t, \sigma_{\Delta t}, s_t, s_m) &= (1 + s_t \Delta \epsilon_{\text{comb}}) \times \\ &\int d\Delta t_{\text{tr}} \mathcal{T}_{\text{comb}}(\Delta t_{\text{tr}}, s_t, s_m) \mathcal{R}_{\text{comb}}(\Delta t - \Delta t_{\text{tr}}, \sigma_{\Delta t}), \end{aligned} \quad (17)$$

where $\mathcal{R}_{\text{comb}}(\Delta t - \Delta t_{\text{tr}}, \sigma_{\Delta t})$ is the 3-Gaussian resolution function and

$$\begin{aligned} \mathcal{T}_{\text{comb}}(\Delta t_{\text{tr}}, s_t, s_m) &= \frac{e^{-|\Delta t_{\text{tr}}|/\tau_{\text{comb}}}}{4\tau_{\text{comb}}} \left\{ 1 - s_t \Delta \omega'_{\text{comb}} \right. \\ &+ s_m \Omega_{\text{comb}} + s_m (1 - 2\omega'_{\text{comb}}) \cos(\Delta m_{\text{comb}} \Delta t_{\text{tr}}) \\ &\left. - \mathcal{S}_{\text{comb}} \sin(\Delta m_{\text{comb}} \Delta t_{\text{tr}}) \right\}, \end{aligned} \quad (18)$$

with

$$\begin{aligned} \mathcal{S}_{\text{comb}} &= (1 - 2\omega'_{\text{comb}}) (s_t a_{\text{comb}} + s_m c_{\text{comb}}) \\ &+ s_t s_m b_{\text{comb}} (1 - s_t \Delta \omega'_{\text{comb}}). \end{aligned} \quad (19)$$

As in the case of $\mathcal{T}_{D^*\rho}$, the weak phase parameters of the peaking and combinatoric background (a_{peak} , b_{peak} , c_{peak} and a_{comb} , b_{comb} , c_{comb}) are set to 0 and are later varied to evaluate systematic uncertainties. Parameters labeled with superscripts “peak” or “comb” are empirical

and thus do not necessarily correspond to physical parameters. In general, their values may be different from those of the $D^*\pi$ -labeled parameters.

The PDF $\mathcal{T}_{q\bar{q}}$ for the continuum background is the sum of two components, one with a finite lifetime and one with zero lifetime:

$$\begin{aligned} \mathcal{T}'_{q\bar{q}}(\Delta t, \sigma_{\Delta t}, s_t) &= (1 + s_t \Delta \epsilon_{q\bar{q}}) \int d\Delta t_{\text{tr}} \mathcal{T}_{q\bar{q}}(\Delta t_{\text{tr}}, s_t, s_m) \\ &\times \mathcal{R}_{q\bar{q}}(\Delta t - \Delta t_{\text{tr}}, \sigma_{\Delta t}), \end{aligned} \quad (20)$$

with

$$\begin{aligned} \mathcal{T}_{q\bar{q}}(\Delta t_{\text{tr}}, s_t) &= (1 - f_{q\bar{q}}^\delta) \frac{e^{-|\Delta t_{\text{tr}}|/\tau_{q\bar{q}}}}{4\tau_{q\bar{q}}} (1 - s_t \Delta \omega_{q\bar{q}}) \\ &+ f_{q\bar{q}}^\delta \delta(\Delta t_{\text{tr}}), \end{aligned} \quad (21)$$

where $f_{q\bar{q}}^\delta$ is the fraction of zero-lifetime events.

4. Resolution Function Parameterization

The resolution function for events of type i and optional secondary type j ($j = \{\text{dir, cas, miss}\}$ for lepton-tagged signal events and $j = \{+, 0\}$ for the peaking and combinatoric $B\bar{B}$ background types) is parameterized as the sum of three Gaussians:

$$\begin{aligned} \mathcal{R}_i^j(t_r, \sigma_{\Delta t}) &= f_i^{nj} \mathcal{G}_i^{nj}(t_r, \sigma_{\Delta t}) \\ &+ (1 - f_i^{nj} - f_i^{oj}) \mathcal{G}_i^{wj}(t_r, \sigma_{\Delta t}) \\ &+ f_i^{oj} \mathcal{G}_i^{oj}(t_r, \sigma_{\Delta t}), \end{aligned} \quad (22)$$

where $t_r = \Delta t - \Delta t_{\text{tr}}$ is the residual of the Δt measurement, and \mathcal{G}_i^{nj} , \mathcal{G}_i^{wj} , and \mathcal{G}_i^{oj} are the “narrow”, “wide”, and “outlier” Gaussians. The narrow and wide Gaussians have the form

$$\begin{aligned} \mathcal{G}_i^{kj}(t_r, \sigma_{\Delta t}) &\equiv \frac{1}{\sqrt{2\pi} s_i^{kj} \sigma_{\Delta t}} \times \\ &\exp \left(-\frac{(t_r - b_i^{kj} \sigma_{\Delta t})^2}{2(s_i^{kj} \sigma_{\Delta t})^2} \right), \end{aligned} \quad (23)$$

where the index k takes the values $k = n, w$ for the narrow and wide Gaussians, and b_i^{kj} and s_i^{kj} are parameters determined by fits, as described in Sec. III G. The outlier Gaussian has the form

$$\mathcal{G}_i^{oj}(t_r, \sigma_{\Delta t}) \equiv \frac{1}{\sqrt{2\pi} s_i^{oj}} \exp \left(-\frac{(t_r - b_i^{oj})^2}{2(s_i^{oj})^2} \right), \quad (24)$$

where in all nominal fits the values of b_i^{oj} and s_i^{oj} are fixed to 0 ps and 8 ps, respectively, and are later varied to evaluate systematic errors.

G. Analysis Procedure

The analysis is carried out with a series of unbinned maximum-likelihood fits, performed simultaneously on the on- and off-resonance data samples and independently for the lepton-tagged and kaon-tagged events. The analysis proceeds in four steps:

1. In the first step, we determine the parameters $f_{D^*\rho} + f_{D^*\pi}$, f_{peak} , and f_{comb} of Eq. (4). In order to reduce the reliance on the simulation, we also obtain in the same fit the parameters $f_{q\bar{q}}^{\hat{G}}$ of Eq. (6), $\epsilon_{q\bar{q}}$ of Eq. (8), σ_L for the signal m_{miss} PDF (Eq. (7)), and all the parameters of the Fisher discriminant PDFs. This is done by fitting the data with the PDF

$$\mathcal{P}_i = \mathcal{M}_i(m_{\text{miss}}) \mathcal{F}_i(F), \quad (25)$$

instead of Eq. (5); i.e. by ignoring the time dependence. The fraction $f_{q\bar{q}}$ of continuum events is determined from the off-resonance sample and its integrated luminosity relative to the on-resonance sample. All other parameters of the \mathcal{M}_i PDFs and the value of $f_{D^*\pi}/(f_{D^*\pi} + f_{D^*\rho}) = 0.87 \pm 0.03$ are obtained from the MC simulation.

2. In the second step, we repeat the fit of the first step for data events with $\cos\theta_T \geq C_T$, to obtain the fraction of signal events in that sample. Given this fraction and the relative efficiencies for direct, cascade, and missing- D signal events to satisfy the $\cos\theta_T < C_T$ requirement, we calculate $f_{D^*\pi}^{\text{miss}} = 0.011 \pm 0.001$ for lepton-tagged events and $f_{D^*\pi}^{\text{miss}} = 0.055 \pm 0.001$ for kaon-tagged events. We also calculate the value of $\rho_{D^*\pi}$ from the fractions of mixed and unmixed signal events in the $\cos\theta_T \geq C_T$ sample relative to the $\cos\theta_T < C_T$ sample.
3. In the third step, we fit the data events in the sideband $1.81 < m_{\text{miss}} < 1.84 \text{ GeV}/c^2$ with the 3-dimensional PDFs of Eq. (5). The parameters of $\mathcal{M}_i(m_{\text{miss}})$ and $\mathcal{F}_i(F)$, and the fractions f_i are fixed to the values obtained in the first step. From this fit we obtain the parameters of $\mathcal{T}'_{\text{comb}}$, as well as those of $\mathcal{T}'_{q\bar{q}}$.
4. In the fourth step, we fix all the parameter values obtained in the previous steps and fit the events in the signal region $m_{\text{miss}} > 1.845 \text{ GeV}/c^2$, determining the parameters of $\mathcal{T}'_{D^*\pi}$ and $\mathcal{T}'_{q\bar{q}}$. Simulation studies show that the parameters of $\mathcal{T}'_{\text{comb}}$ are independent of m_{miss} , enabling us to obtain them in the sideband fit (step 3) and then use them in the signal-region fit. The same is not true of the $\mathcal{T}'_{q\bar{q}}$ parameters; hence they are free parameters in the signal-region fit of the last step. The parameters of $\mathcal{T}'_{\text{peak}}$ are obtained from the MC simulation.

IV. RESULTS

The fit of step 1 finds 18710 ± 270 signal $B \rightarrow D^{*\mp}\pi^\pm$ events in the lepton-tag category and 70580 ± 660 in the kaon-tag category. The m_{miss} and F distributions for data are shown in Figs. 2 and 3, with the PDFs overlaid.

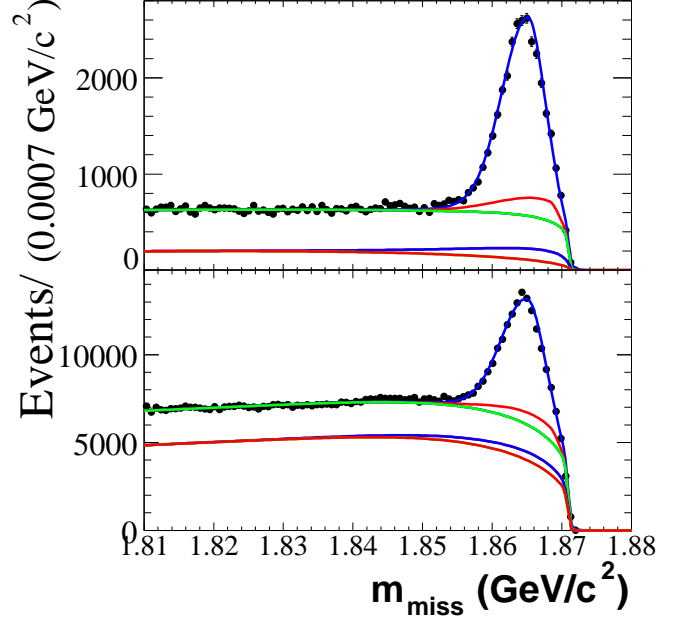


FIG. 2: The m_{miss} distributions for on-resonance lepton-tagged (top) and kaon-tagged (bottom) data. The curves show, from bottom to top, the cumulative contributions of the continuum, peaking $B\bar{B}$, combinatoric $B\bar{B}$, $B \rightarrow D^{*+}\rho^\pm$, and $B \rightarrow D^{*+}\pi^\pm$ PDF components.

The results of the signal region fit (fourth step) are summarized in Table I, and the plots of the Δt distributions for the data are shown in Fig. 4 for the lepton-tagged and the kaon-tagged events. The goodness of the fit has been verified with the Kolmogorov-Smirnov test and by comparing the likelihood obtained in the fit with the likelihood distribution of many parameterized MC experiments generated with the PDF's obtained in the fit on the data. Fig. 5 shows the raw, time-dependent CP asymmetry

$$A(\Delta t) = \frac{N_{s_t=1}(\Delta t) - N_{s_t=-1}(\Delta t)}{N_{s_t=1}(\Delta t) + N_{s_t=-1}(\Delta t)}. \quad (26)$$

In the absence of background and with high statistics, perfect tagging, and perfect Δt measurement, $A(\Delta t)$ would be a sinusoidal oscillation with amplitude $a_{D^*\pi}$. For presentation purposes, the requirements $m_{\text{miss}} > 1.855 \text{ GeV}/c^2$ and $F < 0$ were applied to the data plotted in Figs. 4 and 5, in order to reduce the background. These requirements were not applied to the fit sample, so they do not affect our results.

The fitted values of Δm reported in Table I are in good agreement with the world average (0.502 ± 0.007) ps^{-1}

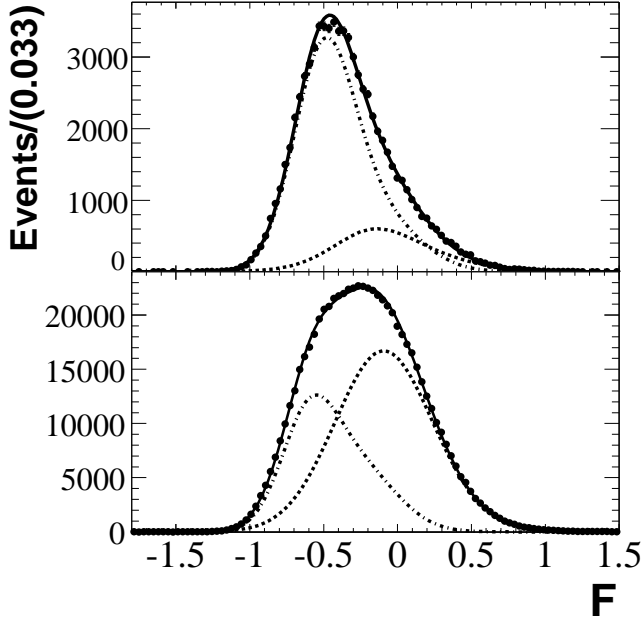


FIG. 3: The F distributions for on-resonance lepton-tagged (top) and kaon-tagged (bottom) data. The contributions of the $B\bar{B}$ (dashed-dotted line) and the continuum (dashed line) PDF components are overlaid, peaking at approximately -0.6 and -0.1 , respectively. The total PDF is also overlaid.

[9]. The fitted values of the B^0 lifetime need to be corrected for a bias observed in the simulated samples, $\Delta\tau = \tau_{fit} - \tau_{gen} = (-0.03 \pm 0.02)$ ps for the lepton-tag and $\Delta\tau = (-0.04 \pm 0.02)$ ps for the kaon-tag events. After this correction, the measured lifetimes, $\tau(B^0) = (1.48 \pm 0.02 \pm 0.02)$ ps and $\tau(B^0) = (1.49 \pm 0.01 \pm 0.04)$ ps for the lepton-tag and kaon-tag, respectively, are in reasonable agreement with the world average $\tau(B^0) = (1.536 \pm 0.014)$ ps [9]. The correlation coefficients of $a_{D^*\pi}^\ell$ ($c_{D^*\pi}^\ell$) with Δm and $\tau(B^0)$ are -0.021 and 0.019 (-0.060 and -0.056).

V. SYSTEMATIC STUDIES

The systematic errors are summarized in Table II. Each item below corresponds to the item with the same number in Table II.

1. The statistical errors from the fit in Step 1 are propagated to the final fit. This also includes the systematic errors due to possible differences between the PDF line shape and the data points.
2. The statistical errors from the m_{miss} sideband fit (Step 3) are propagated to the final fit (Step 4).
- 3-4. The statistical errors from the Step 2 fits are propagated to the final fit.

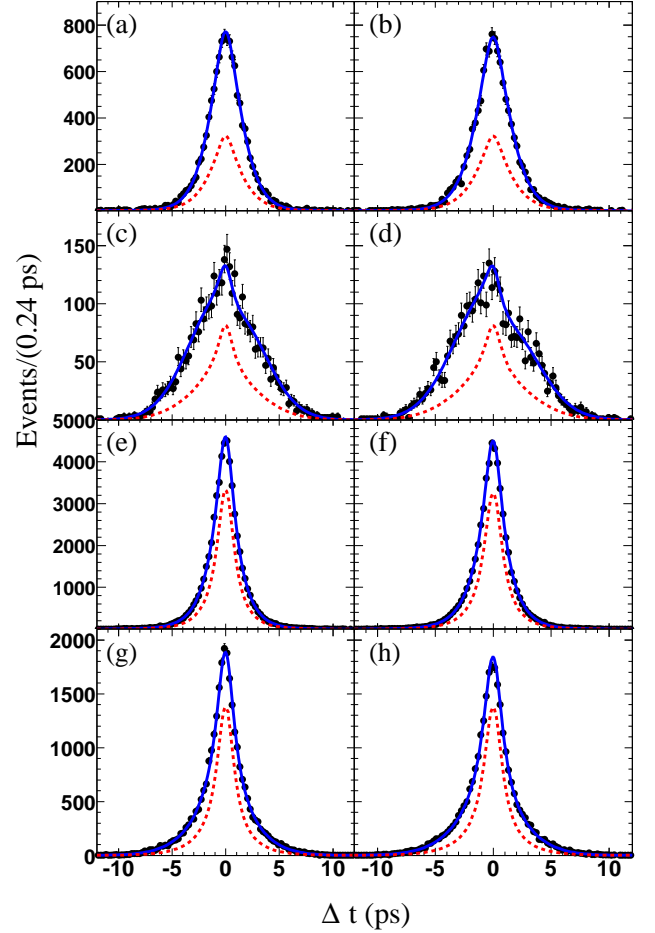


FIG. 4: Δt distributions for the lepton-tagged (a-d) and kaon-tagged (e-h) events separated according to the tagged flavor of B_{tag} and whether they were found to be mixed or unmixed: a,e) B^0 unmixed, b,f) \bar{B}^0 unmixed, c,g) B^0 mixed, d,h) \bar{B}^0 mixed. The solid curves show the PDF, calculated with the parameters obtained by the fit. The PDF for the total background is shown by the dashed curves.

5. The statistical errors associated with the parameters obtained from MC are propagated to the final fit. In addition, the full analysis has been performed on a simulated sample to check for a possible bias in the weak phase parameters measured. No statistically significant bias has been found and the statistical uncertainty of this test has been assigned as a systematical error.
6. The effect of uncertainties in the beam-spot size on the vertex constraint is estimated by increasing the beam spot size by $50 \mu\text{m}$.
7. The effect of the uncertainty in the measured length of the detector in the z direction is evaluated by applying a 0.6% variation to the measured values of Δt and $\sigma_{\Delta t}$.

TABLE I: Results of the fit to the lepton- and kaon-tagged events in the signal region $1.845 < m_{\text{miss}} < 1.880$ GeV/ c^2 . Errors are statistical only. See Sections III F 2, III F 3, and III F 4 for the definitions of the symbols used in this table.

Parameter description	Lepton tags		Kaon tags	
	Parameter	Value	Parameter	Value
Signal weak phase par.	$a_{D^*\pi}^\ell$	-0.042 ± 0.019	$a_{D^*\pi}^K$	-0.025 ± 0.020
	$c_{D^*\pi}^\ell$	-0.019 ± 0.022	$b_{D^*\pi}^K$	-0.004 ± 0.010
			$c_{D^*\pi}^K$	-0.003 ± 0.020
Signal Δt PDF	$\Delta m_{D^*\pi}$	0.518 ± 0.010 ps $^{-1}$	$\Delta m_{D^*\pi}$	0.4911 ± 0.0076 ps $^{-1}$
	$\tau_{D^*\pi}$	1.450 ± 0.017 ps	$\tau_{D^*\pi}$	1.449 ± 0.011 ps
	$\omega_{D^*\pi}^{\text{dir}}$	0.010 ± 0.006	$\omega_{D^*\pi}$	0.2302 ± 0.0035
			$\Delta\omega_{D^*\pi}$	-0.0181 ± 0.0068
	$\Delta\epsilon_{D^*\pi}$	0.027 ± 0.010	$\Delta\epsilon_{D^*\pi}$	-0.0070 ± 0.0073
Signal resolution function	$b_{D^*\pi}^{n,\text{cas}}$	-0.58 ± 0.16		
	$b_{D^*\pi}^{w,\text{cas}}$	0.23 ± 2.01		
	$b_{D^*\pi}^{n,\text{dir}}$	0. (fixed)	$b_{D^*\pi}^n$	-0.255 ± 0.013
	$b_{D^*\pi}^{w,\text{dir}}$	0. (fixed)	$b_{D^*\pi}^w$	-2.07 ± 0.48
	$f_{D^*\pi}^{n,\text{dir}}$	0.978 ± 0.008	$f_{D^*\pi}^n$	0.969 ± 0.007
	$f_{D^*\pi}^{o,\text{dir}}$	0. (fixed)	$f_{D^*\pi}^o$	0.000 ± 0.001
	$s_{D^*\pi}^{n,\text{dir}}$	1.080 ± 0.033	$s_{D^*\pi}^n$	1.029 ± 0.023
	$s_{D^*\pi}^{w,\text{dir}}$	5.76 ± 1.44	$s_{D^*\pi}^w$	4.35 ± 0.40
Continuum Δt PDF	$\tau_{q\bar{q}}$	1.26 ± 0.32 ps	$\tau_{q\bar{q}}$	0.707 ± 0.048 ps
	$\omega_{q\bar{q}}$	0.340 ± 0.009	$\omega_{q\bar{q}}^\tau$	0.045 ± 0.022
			$\omega_{q\bar{q}}^\delta$	0.311 ± 0.006
	$f_{q\bar{q}}^\delta$	0.815 ± 0.064	$f_{q\bar{q}}^\delta$	0.820 ± 0.015
Continuum resolution function	$b_{q\bar{q}}^n$	0.026 ± 0.048	$b_{q\bar{q}}^n$	0.017 ± 0.005
	$b_{q\bar{q}}^w$	-0.39 ± 0.23	$b_{q\bar{q}}^w$	-0.043 ± 0.043
	$f_{q\bar{q}}^n$	0.65 ± 0.12	$f_{q\bar{q}}^n$	0.858 ± 0.014
	$f_{q\bar{q}}^o$	0.068 ± 0.014	$f_{q\bar{q}}^o$	0.018 ± 0.001
	$s_{q\bar{q}}^n$	0.929 ± 0.078	$s_{q\bar{q}}^n$	1.064 ± 0.008
	$s_{q\bar{q}}^w$	1.81 ± 0.28	$s_{q\bar{q}}^w$	2.267 ± 0.099

8. To evaluate the effect of possible misalignments in the SVT, signal MC events are reconstructed with different alignment parameters, and the analysis is repeated.
- 9-11. The weak phase parameters of the $B \rightarrow D^{*\mp}\rho^\pm$, peaking, and combinatoric $B\bar{B}$ background are fixed to 0 in the fits. To study the effect of possible interference between $b \rightarrow u\bar{c}d$ and $b \rightarrow \bar{c}ud$ amplitudes in these backgrounds, their weak phase parameters are varied in the range ± 0.04 and the Step-4 fit is repeated. We take the largest variation in each weak phase parameter as its systematic error.
12. In the final fit, we take the values of the parameters of $\mathcal{T}'_{\text{peak}}$ from a fit to simulated peaking $B\bar{B}$ background events. The uncertainty due to this is evaluated by fitting the simulated sample, setting the parameters of $\mathcal{T}'_{\text{peak}}$ to be identical to those of $\mathcal{T}'_{\text{comb}}$.
13. The uncertainty due to possible differences between the Δt distributions for the combinatoric background in the m_{miss} sideband and signal region is evaluated by comparing the results of fitting the simulated sample with the $\mathcal{T}'_{\text{comb}}$ parameters taken from the sideband or the signal region.
14. The ratio $f_{D^*\rho}/f_{D^*\pi}$ is varied by the uncertainty in the corresponding ratio of branching fractions, obtained from Ref. [9].
- ## VI. PHYSICS RESULTS
- Summarizing the values and uncertainties of the weak phase parameters, we obtain the following results from the lepton-tagged sample:
- $$\begin{aligned} a_{D^*\pi}^\ell &= -0.042 \pm 0.019 \pm 0.010, \\ c_{D^*\pi}^\ell &= -0.019 \pm 0.022 \pm 0.013. \end{aligned} \quad (27)$$
- The results from the kaon-tagged sample fits are
- $$\begin{aligned} a_{D^*\pi}^K &= -0.025 \pm 0.020 \pm 0.013, \\ b_{D^*\pi}^K &= -0.004 \pm 0.010 \pm 0.010, \\ c_{D^*\pi}^K &= -0.003 \pm 0.020 \pm 0.015. \end{aligned} \quad (28)$$

TABLE II: Systematic errors in $a_{D^*\pi}^\ell$ and $c_{D^*\pi}^\ell$ for lepton-tagged events and $a_{D^*\pi}^K$, $b_{D^*\pi}^K$, and $c_{D^*\pi}^K$ for kaon-tagged events.

Source	Error ($\times 10^{-2}$)				
	Lepton tags		Kaon tags		
	$a_{D^*\pi}^\ell$	$c_{D^*\pi}^\ell$	$a_{D^*\pi}^K$	$b_{D^*\pi}^K$	$c_{D^*\pi}^K$
1. Step 1 fit	0.04	0.04	0.10	0.04	0.04
2. Sideband statistics	0.08	0.08	0.40	0.12	0.44
3. $f_{D^*\pi}^{\text{miss}}$	0.02	0.02	0.02	negl.	negl.
4. $\rho_{D^*\pi}$	0.02	0.02	0.02	negl.	negl.
5. MC statistics	0.60	0.82	0.68	0.34	0.70
6. Beam spot size	0.10	0.10	0.07	0.13	0.06
7. Detector z scale	0.03	0.03	0.02	negl.	0.03
8. Detector alignment	0.25	0.55	0.25	0.13	0.41
9. Combinatoric background weak phase par.	0.25	0.22	0.80	0.56	0.72
10. Peaking background weak phase par.	0.36	0.38	0.29	0.17	0.27
11. $D^*\rho$ weak phase par.	0.53	0.52	0.57	0.58	0.58
12. Peaking background	0.21	0.31	0.21	0.41	0.31
13. Signal region/sideband difference	negl.	negl.	0.04	0.03	0.05
14. $\mathcal{B}(B \rightarrow D^{*\mp}\rho^\pm)$	0.17	0.33	0.17	0.22	0.33
Total systematic error	1.0	1.3	1.4	1.0	1.5
Statistical uncertainty	1.9	2.2	2.0	1.0	2.0

Combining the results for lepton and kaon tags gives the amplitude of the time-dependent CP asymmetry,

$$\begin{aligned}
 a_{D^*\pi} &= 2r^* \sin(2\beta + \gamma) \cos \delta^* \\
 &= -0.034 \pm 0.014 \pm 0.009,
 \end{aligned} \tag{29}$$

where the first error is statistical and the second is systematic. The systematic error takes into account correlations between the results of the lepton- and kaon-tagged samples coming from the systematic uncertainties related to detector effects, to interference between $b \rightarrow u\bar{c}d$ and $b \rightarrow c\bar{u}d$ amplitudes in the backgrounds and from $\mathcal{B}(B \rightarrow D^{*\mp}\rho^\pm)$. This value of $a_{D^*\pi}$ deviates from zero by 2.0 standard deviations.

Previous results of time-dependent CP asymmetries related to $2\beta + \gamma$ appear in Ref. [5, 14]. This measurement supersedes the results of the partial reconstruction analysis reported in Ref. [5] and improves the precision on $a_{D^*\pi}$ and $c_{D^*\pi}$ with respect to the average of the published results.

We use a frequentist method, inspired by Ref. [15], to set a constraint on $2\beta + \gamma$. To do this, we need a value for the ratio r^* of the two interfering amplitudes. This is done with two different approaches.

In the first approach, to avoid any assumptions on the value of r^* , we obtain the lower limit on $|\sin(2\beta + \gamma)|$ as a function of r^* .

We define a χ^2 function that depends on r^* , $2\beta + \gamma$, and δ^* :

$$\chi^2(r^*, 2\beta + \gamma, \delta^*) = \sum_{j,k=1}^3 \Delta x_j V_{jk}^{-1} \Delta x_k, \tag{30}$$

where Δx_j is the difference between the result of our measurement of $a_{D^*\pi}^K$, $a_{D^*\pi}^\ell$, or $c_{D^*\pi}^\ell$ (Eqs. (28) and (27)) and the corresponding theoretical expressions given by

Eq. (12). We fix r^* to a trial value r^0 . The measurements of $b_{D^*\pi}^K$ and $c_{D^*\pi}^K$ are not used in the fit, since they depend on the unknown values of r' and δ' . The measurement error matrix V is nearly diagonal, and accounts for correlations between the measurements due to correlated statistical and systematic uncertainties. We minimize χ^2 as a function of $2\beta + \gamma$ and δ^* , and obtain χ_{\min}^2 , the minimum value of χ^2 .

In order to compute the confidence level for a given value x of $2\beta + \gamma$, we perform the following procedure:

1. We fix the value of $2\beta + \gamma$ to x and minimize χ^2 as a function of δ^* . We define $\chi_{\min}^{\prime 2}(x)$ to be the minimum value of the χ^2 in this fit, and δ_{toy}^* to be the fitted value of δ^* . We define $\Delta\chi^2(x) \equiv \chi_{\min}^{\prime 2}(x) - \chi_{\min}^2$.
2. We generate many parameterized MC experiments with the same sensitivity as the data sample, taking into account correlations between the observables, expressed in the error matrix V of Eq. (30). To generate the observables $a_{D^*\pi}^K$, $a_{D^*\pi}^\ell$, and $c_{D^*\pi}^\ell$, we use the values $(2\beta + \gamma) = x$, $r^* = r^0$ and $\delta^* = \delta_{\text{toy}}^*$. For each experiment we calculate the value of $\Delta\chi^2(x)$, computed with the same procedure used for the experimental data.
3. We interpret the fraction of these experiments for which $\Delta\chi^2(x)$ is smaller than $\Delta\chi^2(x)$ in the data to be the confidence level (CL) of the lower limit on $(2\beta + \gamma) = x$.

The resulting 90% CL lower limit on $|\sin(2\beta + \gamma)|$ as a function of r^* is shown in Fig. 6. The χ^2 function is invariant under the transformation $2\beta + \gamma \rightarrow \pi/2 + \delta^*$ and $\delta^* \rightarrow \pi/2 - 2\beta + \gamma$. The limit shown in Fig. 6 is always the weaker of these two possibilities.

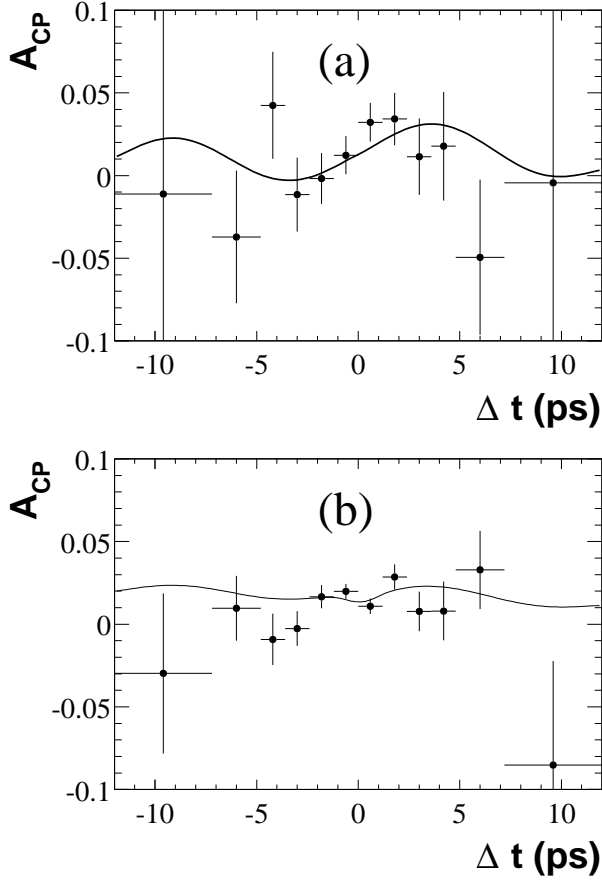


FIG. 5: Raw asymmetry for (a) lepton-tagged and (b) kaon-tagged events. The curves represent the projections of the PDF for the raw asymmetry. A nonzero value of $a_{D^*\pi}$ would show up as a sinusoidal asymmetry, up to resolution and background effects. The offset from the horizontal axis is due to the nonzero values of $\Delta\epsilon_{D^*\pi}$ and $\Delta\omega_{D^*\pi}$.

In the second approach, we estimate r^* as originally proposed in Ref. [2], and assume SU(3) flavor symmetry. With this assumption, r^* can be estimated from the Cabibbo angle θ_C , the ratio of branching fractions $\mathcal{B}(B^0 \rightarrow D_s^{*+}\pi^-)/\mathcal{B}(B^0 \rightarrow D^{*-}\pi^+) = (5.4^{+3.4}_{-3.7} \pm 0.7) \times 10^{-3}$ [16], and the ratio of decay constants $f_{D_s^*}/f_{D^*} = 1.10 \pm 0.02$ [17],

$$r^* = \sqrt{\frac{\mathcal{B}(B^0 \rightarrow D_s^{*+}\pi^-)}{\mathcal{B}(B^0 \rightarrow D^{*-}\pi^+)}} \frac{f_{D^*}}{f_{D_s^*}} \tan(\theta_C), \quad (31)$$

yielding the measured value

$$r^{*\text{meas}} = 0.015^{+0.004}_{-0.006}. \quad (32)$$

This value depends on the value of $\mathcal{B}(D_s^+ \rightarrow \phi\pi^+)$, for which we use our recent measurement [18].

Equation (31) has been obtained with two approximations. In the first approximation, the exchange diagram

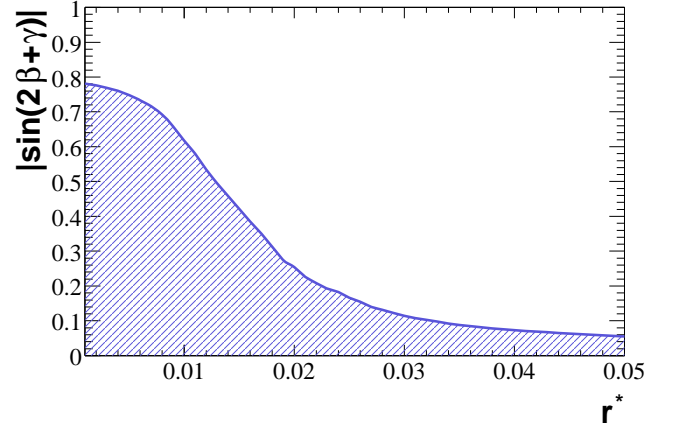


FIG. 6: Lower limit on $|\sin(2\beta + \gamma)|$ at 90% CL as a function of r^* , for $r^* > 0.001$.

amplitude E contributing to the decay $B^0 \rightarrow D^{*+}\pi^-$ has been neglected and only the tree-diagram amplitude T has been considered. Unfortunately, no reliable estimate of the exchange term for these decays exists. The only decay mediated by an exchange diagram for which the rate has been measured is the Cabibbo-allowed decay $B^0 \rightarrow D_s^- K^+$. The average of the *BABAR* and *Belle* branching fraction measurements [16, 19] is $(3.8 \pm 1.0) \times 10^{-5}$. This yields the approximate ratio $\mathcal{B}(B^0 \rightarrow D_s^- K^+)/\mathcal{B}(B^0 \rightarrow D^{*-}\pi^+) \sim 10^{-2}$, which confirms that the exchange diagrams are strongly suppressed with respect to the tree diagrams. Detailed analyses [20] of the $B \rightarrow D\pi$ and $B \rightarrow D^*\pi$ decays in terms of the topological amplitudes conclude that $|E'/T'| = 0.12 \pm 0.02$ for $B^0 \rightarrow D^{*-}\pi^+$ and $|\bar{E}/\bar{T}| < 0.10$ for $B^0 \rightarrow D^{*+}\pi^-$ decays, where E' , \bar{E} and T' , \bar{T} are the exchange and tree amplitudes for these Cabibbo-allowed decays. We assume that a similar suppression holds for the Cabibbo-suppressed decays considered here.

The second approximation involves the use of the ratio of decay constants $f_{D^*}/f_{D_s^*}$ to take into account SU(3) breaking effects and assumes factorization. We attribute a 30% relative error to the theoretical assumptions involved in obtaining the value of r^* of Eq. (32), and use it as described below.

We add to the χ^2 of Eq. (30) the term $\Delta^2(r^*)$ that takes into account both the Gaussian experimental errors of Eq. (32) and the 30% theoretical uncertainty according to the prescription of Ref. [21]:

$$\Delta^2(r^*) = \begin{cases} \left(\frac{r^* - 1.3 r^{*\text{meas}}}{0.004} \right)^2, & \xi_{r^*} > 0.3, \\ 0, & |\xi_{r^*}| \leq 0.3, \\ \left(\frac{r^* - 0.7 r^{*\text{meas}}}{0.006} \right)^2, & \xi_{r^*} < -0.3, \end{cases} \quad (33)$$

where $\xi_{r^*} \equiv (r^* - r^{*\text{meas}})/r^{*\text{meas}}$.

To obtain the confidence level we have repeated the procedure described above with the following changes.

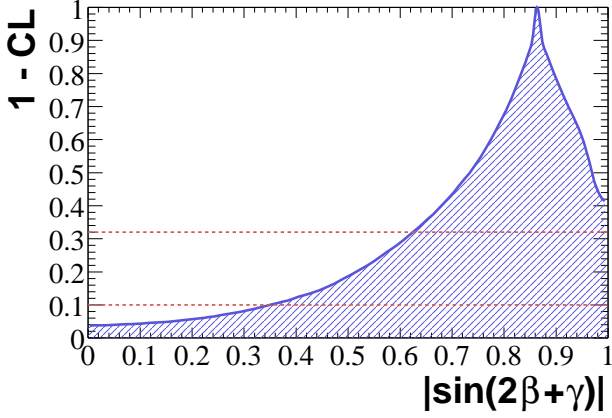


FIG. 7: The shaded region denotes the allowed range of $|\sin(2\beta + \gamma)|$ for each confidence level. The horizontal lines show, from top to bottom, the 68% and 90% CL.

To compute χ^2_{min} we minimize χ^2 as a function of $2\beta + \gamma$, r^* and δ^* . The value $\chi^2_{min}(x)$ is obtained minimizing χ^2 as a function of r^* and δ^* , having fixed $2\beta + \gamma$ to a given value x . We define δ^*_{toy} and r^*_{toy} to be the fitted value of δ^* and r^* in this fit. To generate the observables $a_{D^*\pi}^K$, $a_{D^*\pi}^\ell$, and $c_{D^*\pi}^\ell$ in the parameterized MC experiments, we use the values $(2\beta + \gamma) = x$, $r^* = r^*_{toy}$ and $\delta^* = \delta^*_{toy}$.

The confidence level as a function of $|\sin(2\beta + \gamma)|$ is shown in Fig. 7. We set the lower limits $|\sin(2\beta + \gamma)| > 0.62$ (0.35) at 68% (90%) CL. The implied probability contours for the apex of the unitarity triangle, parameterized in terms of $\bar{\rho}$ and $\bar{\eta}$ defined in Ref. [4], appear in Fig. 8.

VII. SUMMARY

We present a measurement of the time-dependent CP asymmetries in a sample of partially reconstructed $B^0 \rightarrow D^{*\pm}\pi^-$ events. In particular, we have measured the parameters related to $2\beta + \gamma$ to be

$$\begin{aligned} a_{D^*\pi} &= 2r^* \sin(2\beta + \gamma) \cos \delta^* \\ &= -0.034 \pm 0.014 \pm 0.009 \end{aligned} \quad (34)$$

and

$$\begin{aligned} c_{D^*\pi}^\ell &= 2r^* \cos(2\beta + \gamma) \sin \delta^* \\ &= -0.019 \pm 0.022 \pm 0.013, \end{aligned} \quad (35)$$

where the first error is statistical and the second is systematic. We extract limits as a function of the ratio r^* of the $b \rightarrow u\bar{c}d$ and $b \rightarrow \bar{c}ud$ decay amplitudes. With some theoretical assumptions, we interpret our results in terms of the lower limits $|\sin(2\beta + \gamma)| > 0.62$ (0.35) at 68% (90%) CL.

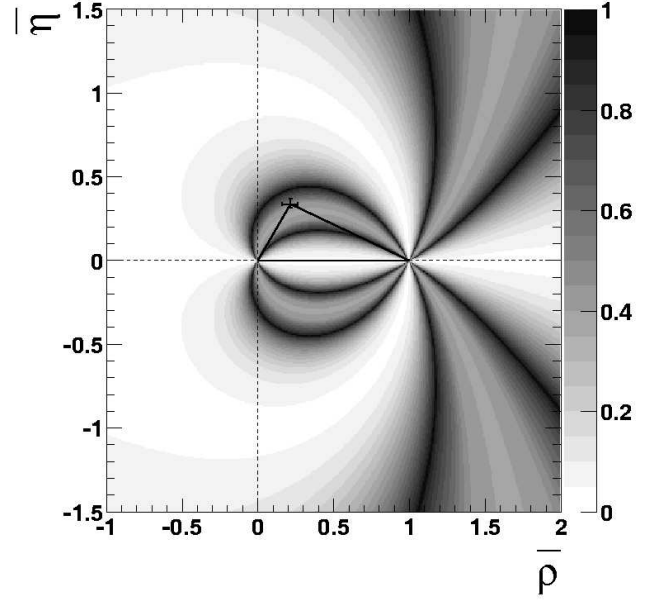


FIG. 8: Contours of constant probability (color-coded in percent) for the position of the apex of the unitarity triangle to be inside the contour, based on the results of Fig. 7. The cross represents the value and errors on the position of the apex of the unitarity triangle from the CKMFitter fit using the “ICHEP04” results excluding this measurement [22].

VIII. ACKNOWLEDGMENTS

We are grateful for the extraordinary contributions of our PEP-II colleagues in achieving the excellent luminosity and machine conditions that have made this work possible. The success of this project also relies critically on the expertise and dedication of the computing organizations that support *BABAR*. The collaborating institutions wish to thank SLAC for its support and the kind hospitality extended to them. This work is supported by the US Department of Energy and National Science Foundation, the Natural Sciences and Engineering Research Council (Canada), Institute of High Energy Physics (China), the Commissariat à l’Energie Atomique and Institut National de Physique Nucléaire et de Physique des Particules (France), the Bundesministerium für Bildung und Forschung and Deutsche Forschungsgemeinschaft (Germany), the Istituto Nazionale di Fisica Nucleare (Italy), the Foundation for Fundamental Research on Matter (The Netherlands), the Research Council of Norway, the Ministry of Science and Technology of the Russian Federation, and the Particle Physics and Astronomy Research Council (United Kingdom). Individuals have received support from CONACyT (Mexico), the A. P. Sloan Foundation, the Research Corporation, and the Alexander von Humboldt Foundation.

-
- [1] N. Cabibbo, Phys. Rev. Lett. **10**, 531 (1963); M. Kobayashi and T. Maskawa, Prog. Theoret. Phys. **49**, 652 (1973).
 - [2] I. Dunietz, Phys. Lett. B **427**, 179 (1998).
 - [3] BABAR Collaboration, B. Aubert *et al.*, Phys. Rev. Lett. **89**, 201802 (2002); BABAR Collaboration, B. Aubert *et al.*, hep-ex/0408127, submitted to Phys. Rev. Lett.; Belle Collaboration, K. Abe *et al.*, Phys. Rev. D **66**, 071102 (2002).
 - [4] L. Wolfenstein, Phys. Rev. Lett. **51**, 1945 (1983).
 - [5] BABAR Collaboration, B. Aubert *et al.*, Phys. Rev. Lett. **92**, 251802 (2004).
 - [6] BABAR Collaboration, B. Aubert *et al.*, Phys. Rev. D **67**, 091101 (2003).
 - [7] GEANT4 Collaboration, S. Agostinelli *et al.*, Nucl. Instrum. Meth. A **506**, 250 (2003).
 - [8] BABAR Collaboration, B. Aubert *et al.*, Nucl. Instrum. Meth. A **479**, 1 (2002).
 - [9] Particle Data Group, S. Eidelman *et al.*, Phys. Lett. B **592**, 1 (2004).
 - [10] G. Fox and S. Wolfram, Phys. Rev. Lett. **41**, 1581 (1978).
 - [11] R. A. Fisher, Annals of Eugenics **7**, 179 (1936); M.S. Srivastava and E.M. Carter, “An Introduction to Applied Multivariate Statistics”, North Holland, Amsterdam (1983).
 - [12] ARGUS Collaboration, H. Albrecht *et al.*, Phys. Lett. B **254**, 288 (1991).
 - [13] O. Long, M. Baak, R.N. Cahn, and D. Kirkby, Phys. Rev. D **68**, 034010 (2003).
 - [14] BABAR Collaboration, B. Aubert *et al.*, Phys. Rev. Lett. **92**, 251801 (2004); Belle Collaboration, T. Sarangi *et al.*, Phys. Rev. Lett. **93**, 031802 (2004).
 - [15] G. Feldman and R. Cousins, Phys. Rev. D **57**, 3873 (1998).
 - [16] BABAR Collaboration, B. Aubert *et al.*, Phys. Rev. Lett. **90**, 181803 (2003).
 - [17] D. Becirevic, Nucl. Phys. Proc. Suppl. **94**, 337 (2001).
 - [18] BABAR Collaboration, B. Aubert *et al.*, hep-ex/0408040, submitted to Phys. Rev. Lett.
 - [19] Belle Collaboration, P. Krokovny *et al.*, Phys. Rev. Lett. **89**, 231804 (2002).
 - [20] C.W. Chiang and J.L. Rosner, Phys. Rev. D **67**, 074013 (2003); C.S. Kim, S. Oh, and C. Yu, hep-ph/0412418.
 - [21] A. Höcker *et al.*, Eur. Phys. J. C **21**, 225 (2001).
 - [22] J. Charles *et al.* (CKMFitter Group), hep-ph/0406184 (to appear in Eur. Phys. J. C).